Available online at www.sciencedirect.com
SCIENCE DIRECT®
ELSEVIER
Nuclear Instruments and Methods in Physics Research A 545 (2005) 330–338
NUCLEAR INSTRUMENTS & METHODS IN PHYSICS RESEARCH Section A
www.elsevier.com/locate/nima

Time-of-flight diffraction with multiple frame overlap Part II: The strain scanner POLDI at PSI

U. Stuhr*, H. Spitzer, J. Egger, A. Hofer, P. Rasmussen, D. Graf, A. Bollhalder, M. Schild, G. Bauer, W. Wagner

Paul Scherrer Institut, Spallation Source Division, CH-5232 Villigen PSI, Switzerland

Received 9 November 2004; received in revised form 21 January 2005; accepted 21 January 2005
Available online 22 April 2005

Abstract

POLDI (Pulse-OverLap DIffractometer) is a multiple pulse-overlap diffractometer at PSI, which is designed mainly for strain-scanning experiments. The multiple pulse-overlap method made it possible to build a time-of-flight diffractometer at a continuous neutron source with short flight path, high resolution and high intensity. The best achievable resolutions for the relative linewidths of the Bragg reflections are between 1×10^{-3} and 2×10^{-3}, depending on the lattice spacing. The layout of the instrument and the features of the chopper, the neutron mirror and the ^{3}He detector in time-focusing geometry are presented. The overall performance of the instrument is discussed with examples of strain-field measurements.

PACS: 61.12.Cd; 07.10.Pz

Keywords: Time-of-flight diffractometer; Residual stress; Strain scanner

1. Introduction

PSI operates the continuous spallation neutron source SINQ. Its neutron flux is comparable to a medium-flux reactor, and the instrumentation at SINQ is similar to that of reactor-based sources as well. Since there is a growing interest in engineering and industrial applications of neutrons and in particular in strain-field measurements, it was decided to build a strain scanner at the thermal neutron beam port 1RNT31. In the preceding paper [1], the concept of a multiple pulse-overlap time-of-flight (TOF) diffractometer was presented, which is ideally suited for strain scanning. Following this concept, the instrument POLDI (Pulse-OverLap DIffractometer) was developed, built, and commissioned, and is in routine operation since beginning of 2003.

*Corresponding author. Tel.: +41 56 310 4513.
fax: +41 56 310 3131.
E-mail address: u.stuhr@psi.ch (U. Stuhr).

0168-9002/$ - see front matter © 2005 Elsevier B.V. All rights reserved.
doi:10.1016/j.nima.2005.01.321

For the design of the instrument, some restrictions in space in the existing neutron hall had to be taken into account. This was mainly the available distance between chopper and sample which was limited to a maximum of 12 m. Furthermore, the layout had to comply with the demand from PSI to be capable for measuring highly radioactive samples. In general, the main requirements and boundary conditions for the instrument were high resolution of the order of 10^{-3} (relative linewidth of the Bragg peaks) at a scattering angle of around 90°, limited flight path, suitability for large engineering components as well as for radioactive samples and, of course, best possible performance.

In the following, the layout of the instrument, the design and performance of the main instrument components and the total performance of the instrument are presented.

2. Instrument design

2.1. General layout

The main differences in the design of a TOF diffractometer based on the multiple pulse-overlap method [1] compared to a conventional TOF-diffractometer affects the chopper and the detector. The chopper may have a high duty cycle, generating many short pulses within the TOF of the neutrons. For the detector, resolution in time as well as in scattering angle are required. Both the arrival time of the neutrons and the scattering angle are needed as information for the analysis of the collected data.

In Fig. 1, a sketch of the POLDI instrument is presented. The distance between the choppers and the sample position is about 11.8 m. The concrete shielding is mainly needed for an easier handling of radioactive samples, but also serves as protection of the environment from high-energy neutrons, which are much more intense at a spallation source compared to a reactor source. The position of the second chopper is reserved for a single-slit chopper, which is intended to be used for structure analysis only and is not discussed in this article.

2.2. Chopper

At a pulse-overlap diffractometer, the chopper is one of the most important components which crucially determines the performance of the instrument. The disc-chopper of POLDI runs with a maximum speed of 15,000 rpm. The disc has a diameter of 700 mm, and contains 32 slits, each with a width of 4 mm and a height of 40 mm. This yields a pulse width of 8 μs (full-width at half-maximum (FWHM)) at 15,000 rpm and a duty cycle of 5.8%. The slits are partitioned in four identical sequences of eight slits each. Therefore, at the maximum chopper speed, the cycle time of one sequence is 1 ms. The eight slits within one sequence are pseudo-randomly distributed. Since the total length of the flight path is about 14 m, the pulse width contributes with $\sim 8.6 \times 10^{-4}$ to the relative uncertainty of the time of flight for

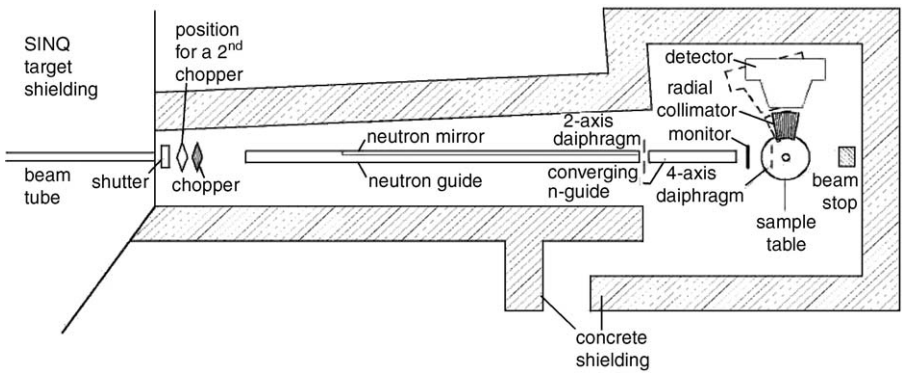

Fig. 1. Sketch of the POLDI instrument. The distance between chopper and sample table corresponds to 11.8 m.

Fig. 2. Picture of the chopper disc. The 32 slits are arranged in four identical sequences with pseudo-random distribution.

neutrons with a wavelength of 2.6 Å. A picture of the chopper disc is shown in Fig. 2.

2.3. Neutron flight path

The shielding of a spallation source has to be much thicker compared to a reactor source; therefore, the beam port at POLDI, between the heavy water moderator and the instrument, is more than 5 m in length. The beam port houses a horizontally and vertically converging steel tube with an exit window of 5.5 mm (width) × 38 mm (height). In order to achieve short chopper pulses and to reduce the background (of fast neutrons and γ-radiation), the width of the beam at the chopper position is small; the slit at the entrance window of the chopper has a width of 4 mm, which is identical to the width of the slits in the chopper disc.

It is important that the neutron optics between chopper and sample minimizes the losses in neutron phase space density, i.e. in the ideal case the neutron density at the chopper should be restored at the sample position. The best way to transmit a narrow neutron beam with minimum losses of neutron density is to image the chopper slit onto the sample, which at POLDI is done by a neutron mirror with an elliptically shaped surface. The length of the mirror is 6 m, which is about half the distance between chopper and sample. The beam height of 40 mm at the chopper, on the other hand, is sufficiently large that for the vertical direction a neutron guide with straight mirrors is well suited to transport the neutrons to the sample. The length of the neutron guide is 10 m. The elliptical mirror is integrated into this guiding section, dividing it into three subsections. In the entrance and exit one, only the plates on top and bottom are coated with Ni/Ti-supermirrors with three times the reflection angle of natural Ni ($m = 3$), whereas the side plates are non-polished glass plates. In the middle section, one side plate forms the elliptical mirror, also coated with $m = 3$ supermirrors. The opposite side consists of straight elements of non-polished glass. The elliptical shape of the mirror is approximated by plates of 500 mm length, each of cylindrical shape and incrementally changing the curvature radii between 560 and 1170 m. The exit section of the neutron guide is build as a vertical 'anti-trumpet' in order to gain some flux at the sample. The horizontal distribution of neutrons at the sample position, in absence of any collimating slits beside the entrance slit of the chopper, is shown in Fig. 3. With running

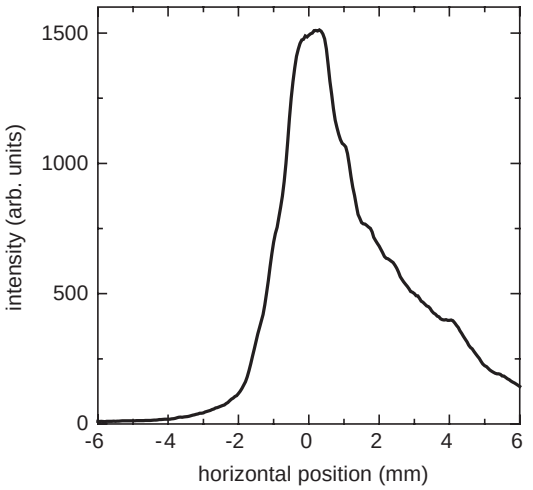

Fig. 3. Intensity distribution at the sample position in the absence of any collimating slits in the flight path.

chopper, the maximum flux in Fig. 3 corresponds to about $6 \times 10^6\,\mathrm{n\,s^{-1}\,cm^{-2}}$.

Beside the conservation of the neutron density, there are other important advantages of an elliptical neutron mirror. The reflection angles at the mirror for all neutrons are about the same. Therefore, neutrons with wavelengths below a well-defined cut-off are not reflected and therefore effectively suppressed. This facilitates the evaluation of the data, since only wavelengths between the cut-off and the Bragg edge have to be taken into account. Fig. 4 shows the wavelength spectrum at the sample position compared to that at the entrance of the neutron guide, which shows that the neutron mirror effectively suppresses all neutrons with wavelengths below 1.15 Å. Furthermore, the neutron mirror avoids any angular or position dependence of the wavelength distribution at the sample position, which is of special importance at a strain scanner.

Two adjustable diaphragms are used to collimate the primary beam. The first one is positioned 3 m in front of the sample in a small gap between the last two sections of the guide/mirror system. It is used to restrict the beam divergence when highest resolution of the instrument is demanded. The second adjustable diaphragm is fixed on an optical bench and can be moved close to the sample. This diaphragm determines the beam size at the sample. Radial collimators in the secondary flight path of the instrument define the extension of the gauge volume perpendicular to the incident beam. At present, three different radial collimators of resolution ~0.6, 1.5 and 4 mm (FWHM) are available at the instrument.

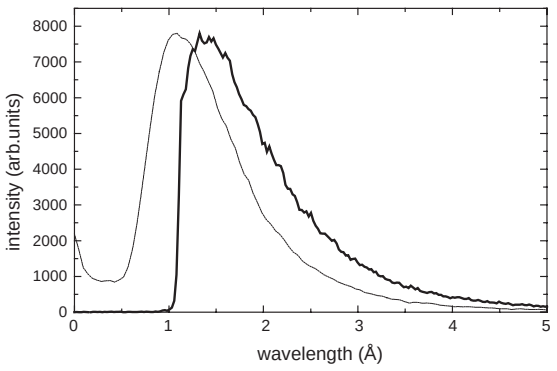

Fig. 4. Comparison of the neutron wavelength distributions at the entrance (dotted line) and at the exit (solid line) of the neutron guide. The spectra are normalized to the same maximum intensity.

2.4. Detector

An one-dimensional position-sensitive ^{3}He-detector was chosen for POLDI, since scintillation detectors with good spatial resolution are expensive and more γ-sensitive. Low γ-sensitivity is important in our case since investigations of highly radioactive samples are foreseen.

Using a gas detector on a TOF diffractometer imposes one severe drawback: the typical thickness of several centimeters for the gas chamber needed for the efficient detection of thermal neutrons makes high-resolution TOF-diffraction difficult or, in combination with short flight paths, nearly impossible when the detector entrance window is perpendicular to the flight direction of the neutrons. With this geometry, the flight time of the neutrons through the counting gas volume causes the major contribution for the uncertainty of TOF determination. At POLDI, for example, the thickness of the ^{3}He volume is 40 mm, which is nearly 0.3% of the total flight path length of the neutrons. Therefore, solely the detector thickness would limit the resolution of the instrument to 0.3%, which is more than a factor of three larger than any other contribution. In the preceding paper [1], it was pointed out that for gas detectors with high spatial resolution time focusing is possible, which eliminates the contribution of the thickness of the gas volume to the instrumental resolution. Time-focusing condition [2] (which means that a geometry is chosen such that the TOF is independent of scattering angle 2θ) is achieved if for each element of the detector an orientation is chosen such that the condition

$$\frac{1}{s}\frac{\partial s}{\partial \theta} = -\cot\,\theta \qquad (1)$$

is fulfilled, where s is the total length of the flight path. This condition imposes that the length of the flight path has to be dependent on the scattering angle. This is only possible if the surface of the detector is not following a line perpendicular to

the flight direction of the neutrons. The same time-focusing condition is applied at some TOF diffractometers which are not using position-sensitive gas detectors. At those instruments, scintillator detectors are used and the orientation of the detector surface has to follow Eq. (1). The situation for a gas detector with high spatial resolution, however, is different: in this case, the orientation of the long side of each detector cell, which will be in general the thickness of the active counting volume, must fulfill the condition of Eq. (1). Therefore, the shape of the detector has to describe a curve, which intersects the curves described by Eq. (1) perpendicular at all scattering angles. A sketch of the scattering geometry and the correct orientation of the detector is given in Fig. 5. The implicit condition for the shape of the detector as derived in Appendix A is given by

$$C\left(\frac{s_c}{r(\theta)}\right)^{1/4}\exp\left(\frac{s_c}{4r(\theta)}\right)=\cos\theta, \qquad (2)$$

where $r(\theta)$ and s_c are the distances between the gauge volume and the detector and chopper, respectively. The $r(\theta)$ can be chosen arbitrarily for a given θ-value. This selection then determines the integration constant C. Fortunately, for scattering angles below about 130°, the shape of the detector, as described by Eq. (2), can very well be approximated by a sector of circle. The POLDI detector is positioned at a distance of about 2 m from the sample, which yields a radius for the detector of about 3m and an angle between detector surface and the direction of the neutron path, which slightly depends on 2θ, of about 73°.

Another problem with large gas detectors at TOF diffractometers arises from the fact that they have to withstand the high gas pressure. Thick neutron windows, however, would not only reduce the efficiency of the detector, but also might give rise to some artefacts in the spectra caused by neutrons scattered in the windows. In order to avoid thick windows at the POLDI-detector, a ^{4}He pressure chamber is attached to the front of the ^{3}He detector chamber. Since both chambers are kept at the same pressure level, a thin Al membrane is sufficient to separate the chambers. The additional window at the entrance of the pressure chamber can also be quite thin, since its area is smaller, and, in contrast to the entrance window of the detector, bending of this window has no influence on the detector performance. A picture of the POLDI detector without shielding is given in Fig. 6.

The detector is a wire detector with two layers of anode wires and three cathode layers. The distances between the layers are 10 mm, which yields a total thickness of 40 mm for the gas volume. Within each anode layer, there are 400 wires in a distance of 2.5 mm for the first layer, in total covering an angular range in 2θ of nearly 30°

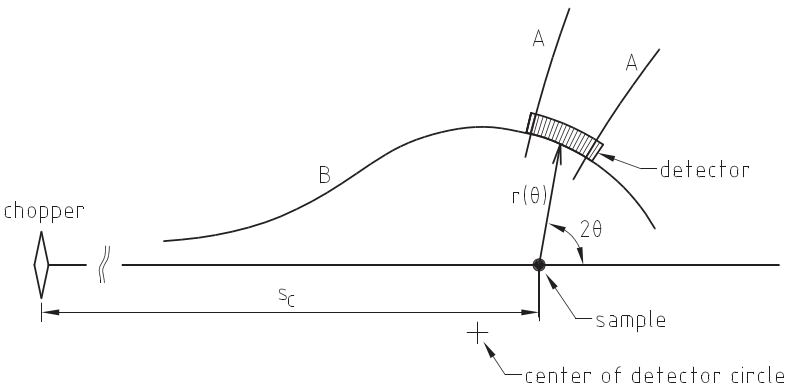

Fig. 5. Sketch of the scattering geometry and the orientation of the ^{3}He detector at POLDI. The neutron detection cells defined by the spatial resolution of the detector and the thickness of the active gas volume are indicated within the detector. The two lines labeled with A describe curves according to Eq. (1) at which, for fixed Q-values, all neutrons have the same time of flight. These lines are parallel to the detector cells. Curve B, defined by Eq. (2), is a line which intersects all constant-Tof curves perpendicularly. It describes the shape and orientation of a gas detector in which all cells are in time-focusing geometry.

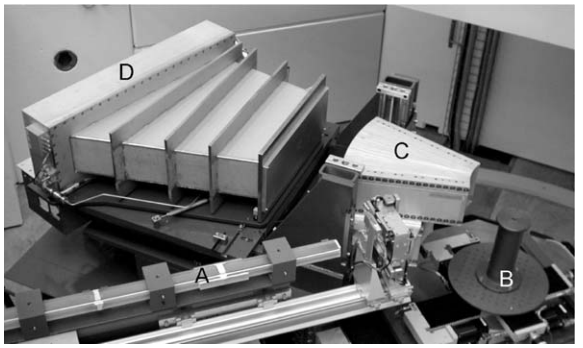

Fig. 6. Top view on the experimental area of POLDI. The picture shows the exit section of the neutron guide, labeled with A, the sample table (B), left from the sample table the radial collimator of 1.5 mm spatial resolution (C) and the detector (D, shielding removed). In front of the detector, the ^{4}He pressure chamber is attached. Note that the detector is not at a measuring position.

at a distance of 2 m from the sample. The distance of the wires in the second anode layer is scaled with the radius of the wire plane. The detector is filled with ^{3}He at 3×10^5 Pa and CF_4 at 1×10^5 Pa, which yields a detector efficiency ranging from 65% for 1.2 Å neutrons to 98% for 4.5 Å neutrons. The internal clock of the detector readout system has a resolution of 0.5 μs. Each event of a detected neutron is labeled with its time and spatial (2θ) information and sent to the histogram memory. The output of the histogram memory is a matrix with the total number of events for each time–2θ channel. The number of time channels can be selected. Typically 500 time channels are used. One time channel then corresponds to 27% of the length of a neutron pulse at the chopper, or, at the highest chopper speed of 15000 rpm, to a time binning of 2 μs. Therefore, the raw data of POLDI are typically stored in a matrix with $400 \times 500 = 200{,}000$ elements.

At POLDI there are two detector positions foreseen, one with the center of the detector at a scattering angle of 90°, the other one at 105°.

3. Performance of the instrument

A first example for POLDI results taken from a Ge powder sample along with the different steps of the data evaluation are given in the preceding paper [1]. The resolution of the instrument for selected chopper speeds and appropriate widths of the first diaphragm are presented in Fig. 7. In this figure, the relative width (FWHM divided by the position of the Bragg peaks) is plotted versus the Q-value, where the momentum transfer Q is $2\pi/d$ and d is the lattice spacing. The measurements were performed with germanium powder for all but one configuration. In the configuration where the best resolution is expected, a $Na_2Ca_3Al_2F_{14}$ powder sample was used, which is known as one of the substances with lowest intrinsic linewidths. The resolution of the instrument in this configuration is between 1.1×10^{-3} and 1.7×10^{-3}, depending on Q, but even when the first diaphragm was opened to 6 mm the resolution still remains below 2×10^{-3} in the entire Q-range of POLDI. All these data have been taken with the detector at the 90° position since this is the most relevant position for strain mapping. At the other detector position at 105° for all configurations, the resolution is about 20% better.

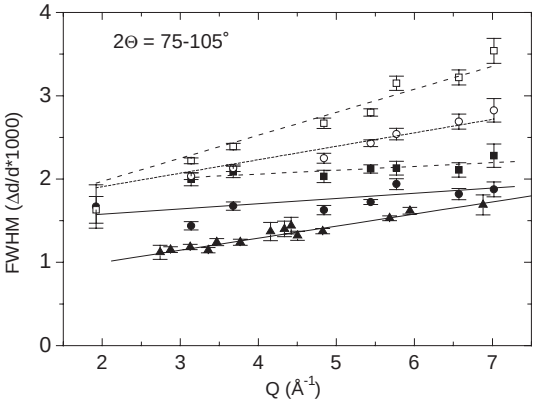

Fig. 7. The resolution of POLDI presented in dependence of the scattering vector Q for selected instrument configurations. The closed symbols are taken with a chopper speed of 15000 rpm, with D1, the width of the first diaphragm 3 m in front of the sample, of 3 mm (triangle), 6 mm (circle) and 10 mm (squares). The open symbols have been measured with $D1 =$ 10 mm and a chopper speed of 10,000 rpm (circles) and 7500 rpm (squares), respectively. The straight lines correspond to the fit results, the data points are the result of the correlation method. The triangles have been taken with $Na_2Ca_3Al_2F_{14}$ powder, all other data with Ge powder.

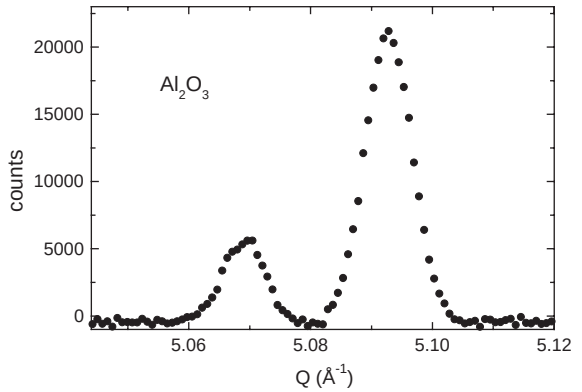

Fig. 8. The double peak of Al_2O_3 around $Q = 5.1\,\text{Å}^{-1}$. These two Bragg reflections do not even overlap although they are separated by less than 0.5%.

As an illustrating example for the resolution of POLDI, the double peak of Al_2O_3 at $Q \approx 5.1\,\text{Å}^{-1}$ is shown in Fig. 8. Since for this substance a considerable intrinsic broadening of the Bragg peaks can be expected, the width of the first diaphragm was chosen to be 6 mm. Although the Q-values of these two peaks differ by less than 0.5%, both peaks are well separated and do not even show an overlap.

4. Examples of strain-scanning experiments

The first step in a strain-scanning experiment is the alignment of the sample. After a first optical pre-alignment the specimen is fixed to the sample table. The precise positions of the surfaces and, if present, interfaces are determined with neutrons. For this purpose the chopper is stopped at an open position, achieving a neutron flux at the sample of about $10^8\,\text{n}\,\text{s}^{-1}\,\text{cm}^{-2}$. The integrated intensity over the whole detector is then determined in dependence on the position of the specimen. Due to the high intensity with the open chopper, the measuring time for each data point does not exceed a few seconds, and the positions of all the surfaces and interfaces even of samples with difficult shapes can be determined with high accuracy in a short time.

Two examples shall illustrate the performance of the instrument in typical strain-scanning experiments. In the first example, a 12 mm thick welded austenitic steel specimen was investigated. The data presented here are taken in the center of the sample at a depth of 6 mm in transmission geometry. The penetration length for the neutrons within the specimen in this configuration is about 17 mm, which corresponds to an attenuation factor of about six for the intensity. Fig. 9 shows the diffractogram calculated from the fit to the raw data. For details of the fitting procedure see Ref. [1]. In the upper part of the figure, the complete diffractogram is shown as the sum of the fit result and the residuals. In the lower part of the figure, two reflections are shown on an enlarged scale, where the fit result is shown as thin line and the data points represent the sum of fit and residuals. These data were taken within 20 min, with the gauge volume (the investigated volume) within the sample being $1.5 \times 1.5 \times 10\,\text{mm}^3$ (about $23\,\text{mm}^3$). All reflections are fitted individually. Therefore, for each of the reflections from a measured spectrum we get a value for the lattice parameter. The relative statistical errors of the position of the Bragg peaks are between 44×10^{-6} for the (3 1 1)-reflection and 137×10^{-6} for the (2 2 2)-reflection.

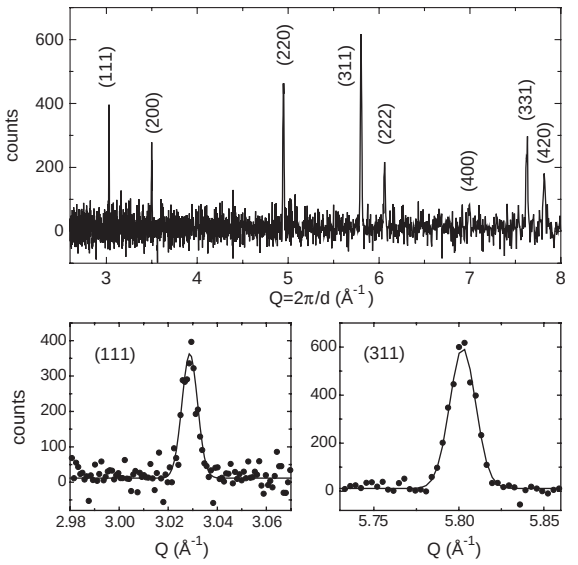

Fig. 9. Diffraction pattern measured from the center of a 12 mm thick steel plate in transmission geometry. The data have been collected within 20 min with a gauge volume of $23\,\text{mm}^3$. Two reflections are shown on an enlarged scale along with the corresponding fit result (solid line).

In the second example, the region close to the interface of a 0.6 mm thick polycrystalline diamond layer covering a WC hard metal plate of 2 mm thickness was investigated. Both phases have a 10% content of Co as binder. The experiment was performed with low Q resolution but high spatial resolution. The radial collimator with the best resolution was used and the gauge volume was $0.6 \times 0.6 \times 20\,\mathrm{mm}^3$ (about $7\,\mathrm{mm}^3$). Fig. 10 shows spectra measured at different positions relative to the interface. The acquisition time for the lower spectrum was 36 min, for the others 1 h each. The figure demonstrates (i) that spectra of a few mm^3 of the sample can be taken within reasonable times and (ii) that measurements in close vicinity to the interface can be performed due to the good achievable spatial resolution. At a distance of 1 mm (top spectrum) from the interface, the intensity of the diamond reflections are only a few per cent of the intensity in the lower spectrum although the gauge volume in the lower figure was not completely filled since the diamond layer is thinner than the width of the gauge volume.

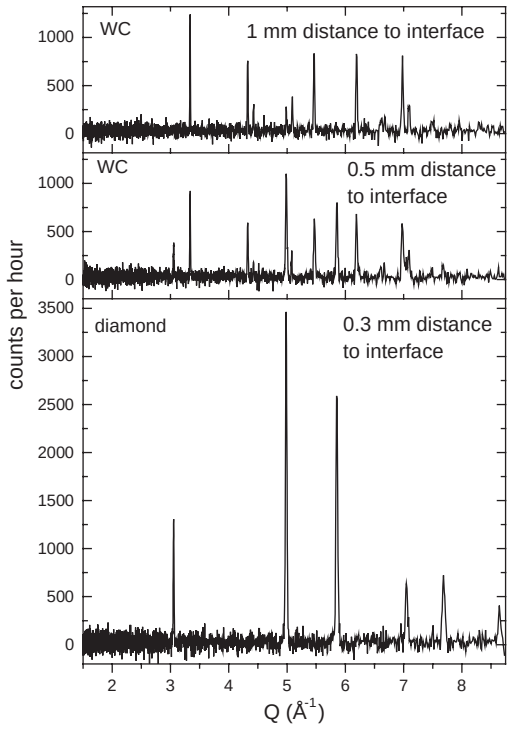

Fig. 10. Results from measurements in close vicinity to the interface between a 0.6 mm polycrystalline diamond layer and a 2 mm tungsten carbide hard metal layer. The experiment was performed at low Q resolution (chopper speed of 5000 rpm) but high spatial resolution. The spectrum in the lower part of the figure was taken within 36 min from the center of the diamond layer. The center and the top spectra were taken from the WC layer at a distance of 0.5 and 1 mm from the interface, respectively.

5. Conclusion

POLDI is a novel type of time-of-flight diffractometer for strain-field scanning at PSI. The high performance of the instrument is demonstrated. The main advantage of this type of instrument is that it can be optimized to high flux and high resolution simultaneously, and that this optimization can be adapted to the requirements of the experiment. The high intensity is achieved by using many pulses of the chopper simultaneously which can be separated by evaluation of the time–2θ pattern of the scattered neutrons. A resolution (FWHM) of better than 2×10^{-3} in the whole Q-range can be achieved at a scattering angle of 90°.

Acknowledgment

We thank Prof. Schreiber for the permission to use his unpublished data of the WC–diamond interface.

Appendix A.

Calculation of the shape of a multiwire gas detector in a time-focusing geometry for each detector cell.

The combination of Bragg's law

$$\lambda = 2d \sin\theta, \tag{A.1}$$

where d is the lattice spacing and θ the Bragg's angle, and the relation between the wavelength λ and the velocity of the neutron v,

$$v = \frac{s}{t_{\mathrm{flight}}} = \frac{2\pi\hbar}{m_{\mathrm{n}}\lambda}, \tag{A.2}$$

where $\hbar$ is Planck's constant, m_n is the mass of the neutrons and s is the length of the total flight path, gives the general equation for the time of flight for the neutrons:

$$t_{\text{flight}} = \frac{2m_n}{\hbar Q} s_{\text{tot}}(\theta) \sin\theta, \tag{A.3}$$

where $Q = 2\pi/d$. The dependence of t_{flight} on Bragg's angle is then given by

$$\frac{\partial t_{\text{flight}}}{\partial\theta} = t_{\text{flight}}\left(\cot\theta + \frac{1}{s_{\text{tot}}}\frac{\mathrm{d}s_{\text{tot}}}{\mathrm{d}\theta}\right). \tag{A.4}$$

If the condition

$$\frac{1}{s}\frac{\partial s}{\partial\theta} = -\cot\theta \tag{A.5}$$

for the dependence of the length of the flight path s on the scattering angle 2θ is fulfilled, then the time of flight is independent on the scattering angle. s will be now replaced by $s_c + s_d$ where s_c is the distance between chopper and sample and s_d is the distance between the sample and the point of detection of the neutron. Using a polar coordination system (s_d, ϕ) with $\phi = 2\theta$, Eq. (A.5) transforms to

$$\frac{1}{s_c + s_d}\frac{\partial s_d}{\partial\varphi} = -\frac{1}{2}\cot\left(\frac{1}{2}\varphi\right). \tag{A.6}$$

In order to achieve time focusing for a given cell of the detector, the orientation of this cell has to be chosen so that its long side within the scattering plane fulfils the condition of Eq. (A.5). Since the spatial resolution of a gas detector typically is much smaller than the thickness of the detector, the surface of the detector has to intersect all the curves, which fulfil the condition of Eq. (A.5), perpendicularly. The condition for perpendicular intersection is given by

$$\frac{1}{r}\frac{\partial r(\varphi)}{\partial\varphi} = -s_d\left(\frac{\partial s_d}{\partial\varphi}\right)^{-1}, \tag{A.7}$$

where the shape of the detector is described by the distance to the sample and the scattering angle $r(2\theta) = r(\phi)$. The combination of Eqs. (A.6) and (A.7) yields

$$\frac{\partial r(\varphi)}{\partial\varphi} = 2\frac{r^2(\varphi)}{s_c + r(\varphi)}\tan\left(\frac{1}{2}\varphi\right), \tag{A.8}$$

where s_d is replaced by $r(\phi)$. The integration of (A.8) leads to

$$\int\left(\frac{1}{r(\varphi)} + \frac{s_c}{r^2(\varphi)}\right)\mathrm{d}r = 2\int\tan\left(\frac{1}{2}\varphi\right)\mathrm{d}\varphi \tag{A.9}$$

and

$$\ln(r(\varphi)) - \frac{s_c}{r(\varphi)} + C_1 = -4\ln\cos\left(\frac{1}{2}\varphi\right) \tag{A.10}$$

and finally to the implicit equation for the shape of the detector $r(\theta)$ to

$$C\left(\frac{s_c}{r(\theta)}\exp\frac{s_c}{r(\theta)}\right)^{1/4} = \cos\theta, \tag{A.11}$$

where $C = s_c^{-1/4}\exp(-C_1/4)$ is the integration constant which can be chosen arbitrarily and determines the distance between sample and detector.

References

[1] U. Stuhr, Nucl. Instr. and Meth. A, this issue, doi:10.1016/j.nima.2005.01.320.
[2] J.M. Carpenter, Nucl. Instr. and Meth. 47 (1967) 179.